Carbon 243 (2025) 120422

Contents lists available at ScienceDirect

Carbon

journal homepage: www.elsevier.com/locate/carbon

Research paper

Room temperature water splitting at the basal plane of graphene grown on nickel

Monica Pozzo [a,b,c,*], Paolo Lacovig [d], Marco Bianchi [d], Monika Schied [d], Luca Bignardi [e], Francesca Zarotti [f,1], Roberto Felici [g], Dario Alfè [c,h,i], Silvano Lizzit [d], Rosanna Larciprete [f,*]

[a] Faculty of Technological & Innovation Sciences, Universitas Mercatorum, Piazza Mattei 10, 00186, Rome, Italy
[b] Institute for Materials Discovery, UCL East, Marshgate Building, 7 Sidings Street, Stratford, London, E20 2AE, UK
[c] Department of Earth Sciences, Thomas Young Center, University College London, 5 Gower Place, London WC1E 6BS, UK
[d] Elettra-Sincrotrone Trieste, S.S. 14 Km 163.5 in AREA Science Park, 34149, Basovizza, Trieste, Italy
[e] Department of Physics, University of Trieste, Via Alfonso Valerio 2, 34127, Trieste, Italy
[f] CNR- Institute for Complex Systems, via dei Taurini 19, 00185, Rome, Italy
[g] CNR-ISM, via del Fosso del Cavaliere 100, 00133, Rome, Italy
[h] Dipartimento di Fisica "Ettore Pancini", Università Federico II, Via Cinthia 21, 80126, Napoli, Italy
[i] London Centre for Nanotechnology, Thomas Young Centre, University College London, 17-19 Gordon Street, London WC1H 0AH, UK

ARTICLE INFO

Keywords:
Water splitting
Graphene
Photoelectron spectroscopy
Surface diffraction
Scanning tunneling microscopy
Density functional theory calculations

ABSTRACT

The initial stage of the interaction of water molecules with graphene supported on Ni(111) was studied by combining electronic, structural and scanning probe microscopy techniques with theoretical calculations. We demonstrate the occurrence of dissociative water adsorption at the basal plane of graphene, which renders the surface evenly covered by H atoms, whereas the OH counterparts are somehow removed from the graphene surface. Density functional theory calculations show that water splitting on Gr/Ni(111) is an endothermic process and becomes exothermic when occurs close to pre-adsorbed H atoms or in correspondence of C vacancies. However, the dissociation energy barrier for uni-molecular dissociation becomes compatible with a reasonable reaction rate at room temperature only when it takes place in correspondence of Ni atoms trapped at the C vacancies during Gr growth. On the other hand, due to the limited number of single Ni atoms catalysts in the Gr layer, it seems reasonable that collective adsorption processes or autocatalytic dissociative reactions are largely responsible for the extensive water dissociation observed experimentally.

1. Introduction

A smart strategy to advance both hydrogen production and storage aims at developing dedicated nanomaterials, featuring a wide variety of morphological structures in comparison to their bulk counterpart and a high specific surface area that expands the storage capacity [1]. Although graphene (Gr) could play a dominant role in this field, actually its use is limited by its chemical neutrality, which often makes it necessary to add heteroatoms (B, N, S, and P) and functional groups and/or create structural defects [2,3] to tune the local charge distribution and induce some reactivity. Such lattice manipulation could enable the direct use of graphene as catalyst for water splitting, since the resultant areas of unbalanced charges help overcome its intrinsic hydrophobic nature. Also the close interaction with a metal support responsible for a strong charge transfer could lead to the formation of a dipole layer capable of catalyzing chemical reactions, and, in this respect, the Gr/Ni(111) interface has often been reported as one of the most reactive Gr/metal systems [4–6]. The Gr-Ni(111) equilibrium distance (2.09–2.17 Å) [7–9] on one hand is large enough to maintain sufficient flexibility in the Gr layer to bind adsorbates [10] and on the other hand is small enough to determine measurable hybridization/charge rearrangement [11] due to the electron injection into the graphene layer [10].

Recently, it was demonstrated that it is possible to achieve water dissociation at room temperature (RT) at the surface of Ni single crystals covered by graphene monolayers [12]. If the Gr/Ni(111) interface is exposed to water doses high enough to have intercalation

* Corresponding authors.
E-mail addresses: monica.pozzo@unimercatorum.it, m.pozzo@ucl.ac.uk (M. Pozzo), rosanna.larciprete@isc.cnr.it (R. Larciprete).
[1] Current address: ENEA, Italian National Agency for New Technologies, Energy and Sustainable Economic Development, Via Enrico Fermi, 45, 00044 Frascati, Rome, Italy.

https://doi.org/10.1016/j.carbon.2025.120422
Received 20 March 2025; Received in revised form 10 May 2025; Accepted 12 May 2025
Available online 28 May 2025

below graphene, a part of the intercalated water molecules dissociate. The H atoms remain stored in the system and are released as H_2 at temperatures of the order of 450 K. It is worth pointing out that on the bare Ni(111) surface water adsorbs molecularly at temperature below 150–170 K, might split in the presence of predosed O or OH or under the action of electron beams [13,14], but requires vibrational excitation to dissociate when impacting the Ni surface at RT [15]. Therefore, the presence of graphene seems to be indispensable to achieve RT water splitting. In the experiment reported in Ref. [12], after the exposure to water, the Gr layer resulted extensively lifted by both intact molecules and their fragments. For this configuration, density functional theory (DFT) calculations showed that the dissociation of intercalated water is facilitated by the presence of Stone–Wales defects in the Gr lattice, which render the molecular dissociation in the space between Gr and the Ni support exothermic. However, this study [12], which was focused on the late reaction stage, did not address the key-question, that is whether the Gr/Ni(111) interface itself possesses intrinsic catalytic activity towards water splitting.

In this study we combined x-ray photoelectron spectroscopy (XPS), thermal programmed desorption (TPD), surface x-ray diffraction and scanning tunneling microscopy (STM) measurements to investigate the early stage of the interaction between water molecules and Gr/Ni(111). Our aim was to achieve a complete definition of the surface reactions leading to hydrogen production and a more precise identification of the ambient conditions which trigger water dissociation on Ni-supported Gr. We experimentally identified the intrinsic activity of the Gr/Ni interface by revealing the hydrogenation of the Gr layer, consequent to the dissociative water chemisorption. Structural measurements and microscopy imaging were used to establish that the splitting reaction occurs on the basal plane of the graphene surface. Then, we used DFT calculations to determine the adsorption energy of intact water and of its fragments on Gr/Ni(111) and the energetics of the dissociation reactions of single water molecules in different interface configurations.

2. Methods

2.1. Experimental section

The XPS and TPD experiments were performed at the SuperESCA beamline of the synchrotron radiation source Elettra (Trieste, Italy). The Ni(111) crystal was mounted on a manipulator capable of providing a precisely controlled rate of sample heating and cooling. The temperature was measured by means of a thermocouple spot-welded on the side of the disk-shaped Ni crystal. Surface cleaning was carried out by repeated sputtering cycles at 1 keV followed by annealing up to 1020 K. The sample quality was checked by means of low-energy electron diffraction (LEED) and by verifying that the spectral features relative to C and O contaminants were absent in the XPS spectra. Graphene was grown by dosing ethylene at 5×10^{-7} mbar onto the Ni(111) surface kept at 870 K. The growth was monitored on line by fast XPS spectroscopy of the C 1s core level. The achievement of complete coverage of the Ni substrate by the Gr monolayer was ensured by prolonging the exposure to ethylene well beyond the saturation of the C1s spectrum intensity, to fill eventual C vacancies not detectable by XPS. The Gr/Ni(111) surface was dosed by letting water flow in the ultra-high vacuum chamber at a pressure of 5×10^{-4} mbar. The samples was exposed to water at room temperature up to a total dose w_d of 7.3 ML (1 ML = 10^6 Langmuir = 1.33 mbar s). During sample dosing the vacuum gauge was kept off to exclude any eventual contribution of the hot filament to water splitting. Adsorbate coverage on graphene is given in monolayers, where 1 $ML_{Gr} = 3.82 \times 10^{15}$ atoms/cm^2, which is the atomic surface density of graphene. High resolution O1s, C1s and valence band spectra were measured at photon energies of 650, 400 and 100 eV, respectively. For each spectrum the binding energy (BE) was calibrated by measuring the Fermi level position of the Ni crystal. XPS measurements were performed with the photon beam impinging at grazing incidence (70°), while photoelectrons were collected at normal emission angle (0°), both angles being considered with respect to the normal to the Ni crystal plane. The core level spectra were best fitted with Doniach-Šunjić functions convoluted with Gaussians, and a linear background. The TPD data were recorded by a quadrupole mass spectrometer equipped with a quartz shield ('Feulner cup' [16]) with a sample-size opening. Before each measurement, the sample was placed in front of the cup, almost in contact with it, and was heated at a rate of 2 K/s.

Surface x-ray diffraction experiments were carried out in the UHV station of the SIXS beamline at the SOLEIL synchrotron radiation facility, Paris Saclay, using a photon energy of 18 keV. Sample cleaning, graphene growth and water dosing were carried out by following the same procedures described above. The surface chemical composition was determined by Auger electron spectroscopy. As reference system for the x-ray measurements we used the hexagonal surface cell of the Ni(111) face. Crystal Truncation Rods (CTRs) were measured along the surface normal direction L in units of $c^\star = 2\pi/c$, $|c| = 6.10$ Å. Structure refinements were conducted using the ROD program based on a least–squares method.

STM measurements were carried out at the CoSMoS facility at Elettra Sincrotrone Trieste. Also in this case sample cleaning, graphene growth and water dosing were carried out by following the same procedures described above. The images were acquired at room temperature with a SPECS STM 150 Aarhus instrument equipped with a W tip.

2.2. Computational methods

Calculations were carried out using spin polarized DFT as implemented in the VASP code [17]. The systems were modeled with a slab with 5 layers of Ni in a 4 × 4 hexagonal supercell and a layer of 4 × 4 unit cells of graphene placed on top. The bottom three layers of Ni were kept frozen at their bulk geometry, with a lattice parameter of 2.492 Å. The rest of the system was fully relaxed using the rev–vdw–DF2 functional [18] until the largest residual force was less than 0.0015 eV/Å. We employed the projector augmented method (PAW) [19] using PBE [20] potentials. The plane wave cut-off was set to 400 eV, and the relaxations were performed by sampling the Brillouin zone using 2 × 2 × 1 k-point grids. Energy barriers were calculated using the nudget elastic band method [21] and 7 images. For the calculation we considered the Gr layer in the *top-fcc* configuration on Ni(111). The adsorption energy E_a of a species X (X = H, OH, H_2O) adsorbed on Gr/Ni(111) is defined as

$$E_a = E_{X/\mathrm{Gr/Ni}} - E_{\mathrm{Gr/Ni}} - E_X$$

where $E_{X/\mathrm{Gr/Ni}}$ is the total energy of the relaxed X/Gr/Ni(111) system and $E_{\mathrm{Gr/Ni}}$ and E_X are the energies of the Gr/Ni(111) substrate and of the isolated X species in the gas phase, respectively. Analogously, in the case of water dissociation, also in the presence of n pre-adsorbed H atoms, the adsorption energy is defined as:

$$E_a = E_{n\mathrm{H+(H+OH)}} - E_{\mathrm{Gr/Ni}} - \frac{n}{2}E_{\mathrm{H_2}} - E_{\mathrm{H_2O}}$$

3. Results and discussion

3.1. Characterization of Gr/Ni(111) exposed to water

Fig. 1a and b show the C1s and O1s spectra measured on the clean Gr/Ni(111) surface and after the exposure to increasing doses of H_2O molecules at RT. The C1s spectrum taken on the clean sample (curve A in Fig. 1a) consists of a main component C_0 at 284.82 eV, arising from the graphene layer strongly interacting with the Ni substrate, with the C atoms occupying predominantly three-fold (*fcc* but also *hcp*) and top sites on the Ni(111) surface [22]. The little shoulder S on the low BE side (284.44 eV) originates from a limited fraction of Gr regions where the interaction with the substrate is much weaker. This

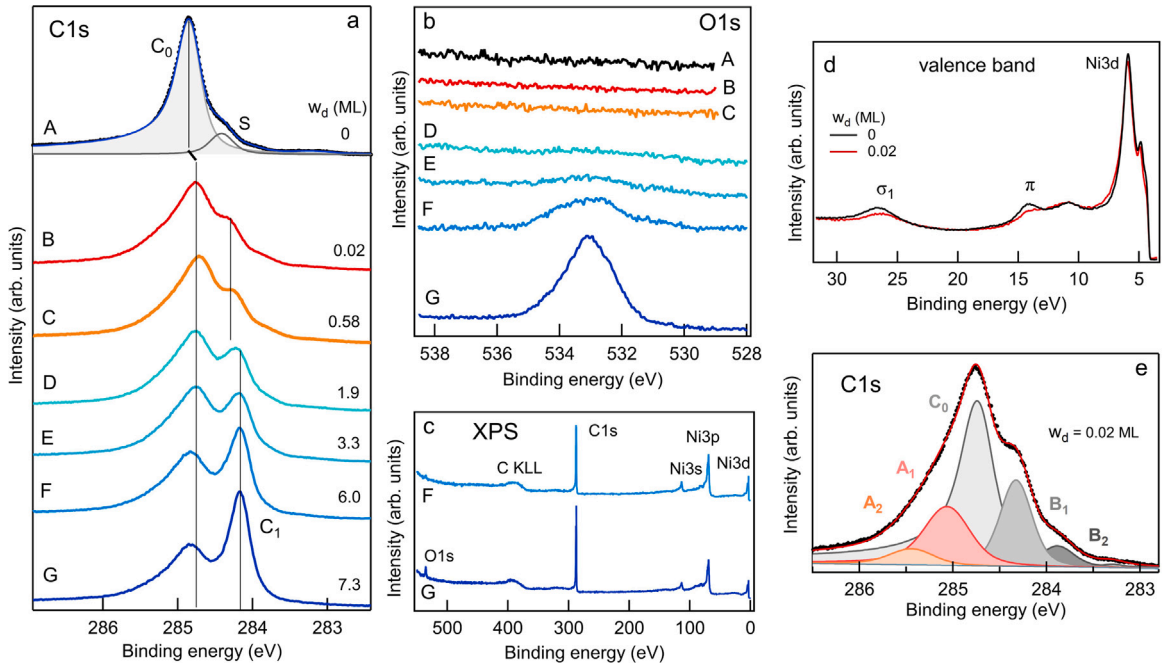

Fig. 1. (a) C1s and (b) O1s core level spectra measured for the clean Gr/Ni(111) surface (curves A) and after the exposure to increasing quantities of water (curves B-G); (c) survey spectra measured after the heaviest water doses, namely w_d = 6.0 ML (curve F) and w_d = 7.3 ML (curve G). Note that H atoms are not detected by XPS; (d) valence band spectra measured on the clean Gr/Ni(111) surface and after w_d = 0.02 ML; (e) Experimental curve (black dots), best fit curve (red line) and spectral components of the C1s spectrum measured for the Gr/Ni(111) surface dosed with 0.02 ML of water (see curve B in Fig. 1a). (A colour version of this figure can be viewed online.)

happens in regions rotated with respect to the (111) orientation of the Ni lattice [23,24] and/or lying on Ni carbide islands rather than on the crystal surface [25].

The exposure to a water dose w_d = 0.022 ML determines strong modifications in the C1s line shape (curve B in Fig. 1a), with some spectral intensity appearing on the low and high BE sides of the main peak, which is itself significantly attenuated and shifted by −100 meV. Interestingly, the corresponding spectrum measured in the O1s region (curve B in Fig. 1b) does not show any signal due to chemisorbed water or its O-containing fragments. Much higher water doses are necessary to observe additional spectroscopic changes. Starting from w_d = 1.9 ML the C1s spectrum shows the appearance of the peak C_1 at ~284.2 eV, a BE position typical for Gr detached from the Ni substrate [12,26–28]. Then, the component C_1 can be taken as a fingerprint for the occurrence of adsorbate intercalation below Gr. Differently, in the O1s region some intensity above the background curve is revealed only after w_d = 3.3 ML (curve E in Fig. 1b). Upon heavier exposure to water, the growth of the O1s peak is accompanied by the increase of the C_1 component intensity in the C1s spectrum, due to the formation of larger Gr regions decoupled from the substrate. However, even after the highest water dose of 7.3 ML, in the wide XPS spectra ($h\nu$ = 650 eV) the O1s intensity remains definitely negligible (see Fig. 1c) in comparison with the dramatic modification of graphene revealed by the C1s line shape. Note that at a photon energy of 650 eV the ratio between the O1s and C1s photoionization cross sections is higher than 2 [29,30].

The case of Gr/Ni(111) extensively lifted after water dosing was discussed in detail in Ref. [12] together with the trend followed during thermal annealing. This late stage, whose results were thoroughly confirmed in this experiment (see Figure S1), will not be discussed further.

It is intriguing to note that the C1s line shape measured for the sample exposed to a low water dose (curve B and C in Fig. 1a) is identical to that measured for the Gr/Ni(111) surface exposed to a low dose of H atoms at RT [27,31]. The spectrum reported in Ref. [27] is shown in Figure S2. The same strong similarity is observed between the corresponding valence band spectra: Fig. 1d shows that the interaction with H_2O leaves the Ni3d band almost unmodified but attenuates, broadens and slightly down-shifts the σ_1 and π bands of graphene, as it happens after the chemisorption of H atoms on Gr/Ni(111) (Figure S3). Hence, both C1s and valence band spectra indicate that the interaction between the Gr/Ni(111) interface and H_2O molecules results in the bonding of H atoms to graphene, which implies the occurrence of water splitting. In light of these observations, as it is shown in Fig. 1e, the C1s spectrum measured for the sample exposed to w_d = 0.02 ML (curve B in Fig. 1a) is best-fitted by using the same components identified for the H/Gr/Ni(111) surface (Figure S2) and attributed by DFT calculations to C atoms directly bonded to H atoms and to their first neighbors [27], in satisfactory agreement with the assignment reported in Ref. [31]. Therefore, C atoms directly bonded to H contribute to A_2 (285.43 eV) (H monomers and dimers) and to A_1 (285.05 eV) (H trimers or larger clusters), whereas graphene sites neighboring C–H bonds originate the B_1 (284.32 eV) (neighbors of one and two C–H bonds) and the B_2 (283.88 eV) (neighbors of three C–H bonds) components. As in the case of the clean Gr/Ni(111), non-hydrogenated C atoms are represented by the component C_0 (284.71 eV), which, however, both for the sample exposed to atomic H and to water, is shifted by about −100 meV with respect to the pristine position, as a consequence of the charge redistribution in the whole Gr layer caused by hydrogenation [27]. As it has been noted above, the C1s line shape measured after w_d = 0.02 ML remains stable when the dose is more than doubled, and then evolves with the appearance of the component C_1, which subtracts intensity from all other components. Hence, the coverage of chemisorbed H saturates at the value reached after the first water dose, which, from the cumulative spectral weight of the components A_1 and A_2 (Fig. 1e) both due to C–H bonds, can be estimated to be ~0.25 ML_{Gr}. Likely, once the maximal coverage of H chemisorbed on Gr/Ni(111) is reached, the impinging water molecules react with the functionalized surface leaving the average number of H atoms bonded to Gr unaltered.

The occurrence of Gr hydrogenation is further proved by the evolution of the C1s spectrum measured while heating the sample and by the corresponding TPD curves, shown in Fig. 2a and b, respectively. Fig. 2a displays the integrated intensity of the C1s components as a function of the sample temperature.

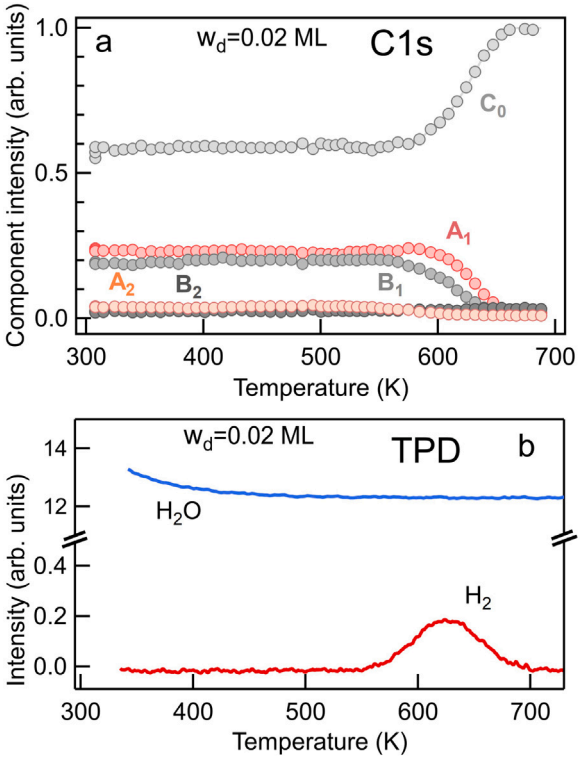

Fig. 2. Thermal evolution of the Gr/Ni(111) surface exposed to a water dose w_d = 0.02 ML: (a) integrated areas of the C1s components (see Fig. 1e) and (b) TPD curves as a function of the annealing temperature.

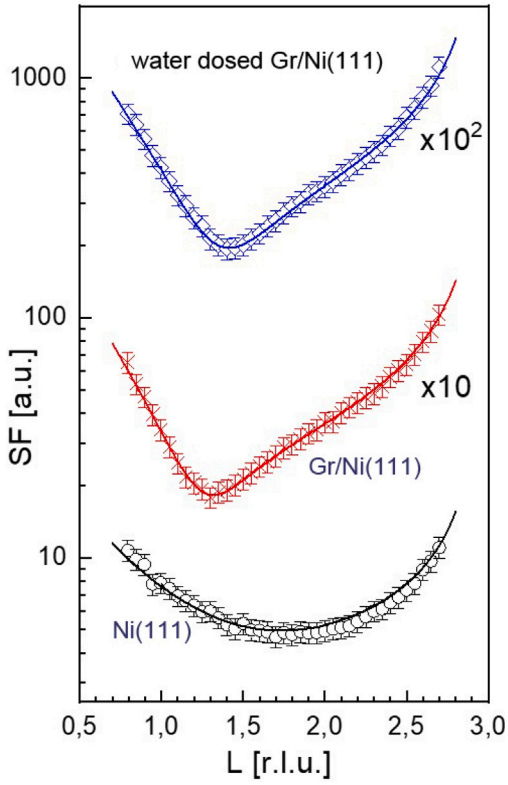

Fig. 3. Structure Factor (SF) as a function of L along the (00L) specular rod for clean Ni (111) (ottom curve), Gr/Ni (111) (middle curve), and Gr/Ni (111) exposed to 0.2 ML of water (top curve). Continuous lines represent the corresponding simulated curves for each system.

It comes out that the A_1 and B_1 peaks start to convert into C_0 around 580 K, which is the typical temperature at which the H_2 molecules, formed after the recombination of two H adatoms, desorb both from the hydrogenated graphite [32] and graphene/Ni [27]. Accordingly, the TPD curve shown in Fig. 2b indicates that the release of H_2 molecules in the gas phase initiates around 580 K [27]. As for the trend shown by the partial pressure of water in the TPD curve (Fig. 2b), only a smooth decay of the background signal is observed, which excludes any measurable specific desorption of water molecules from the sample surface, in agreement with their low adsorption energy on Gr/Ni(111), which will be discussed below.

The demonstration that water molecules are efficiently dissociated at RT without the need to get in direct contact with the Ni surface by intercalating below Gr is provided by x-ray diffraction measurements. The structural modification occurring in the Gr/Ni(111) interface exposed to water molecules was determined by comparing the specular crystal truncation rods (CTRs) measured on the clean Ni crystal and on the Gr/Ni(111) substrate before and after the exposure to w_d = 0.2 ML. The experimental CTRs plotted in Fig. 3 show the structure factor (SF) as a function of L, the momentum transfer perpendicular to the surface expressed in reciprocal lattice units (r.l.u.). The simulated curves obtained in each case are also shown. For the Ni crystal, the experimental data were fitted according to a 111-oriented *fcc* structure (a = b = 2.4890 Å, c = 6.1037 Å, $\alpha = \beta = 90°$, $\gamma = 120°$) with a small outward relaxation in the top layer of 0.03 Å. The Gr layer grown epitaxially on the Ni crystal modifies the shape of the specular rod and shifts the minimum to L = 1.3. After the water dose, the distinctive CTR shape observed for the clean Gr/Ni(111) is smoothed and slightly shifted to higher L values. These curves were best-fitted by assuming the Gr layer in the *top-fcc* configuration on Ni(111). For plain Gr/Ni(111), the model that best reproduced the experimental CRT consists of a Gr layer lying at an average distance d = 2.24 Å from the topmost Ni layer. After exposure to water, the CRT analysis reveals that Gr slightly approaches the substrate reducing the average Gr-Ni separation to 2.12 Å. In this case, the more rounded CRT shape indicates some structural disorder in the interface. The d value we found for clean Gr/Ni(111), which is higher than the distance calculated (2.09–2.17 Å) [7,8] for *top-fcc* Gr on Ni(111) and measured (2.088 Å) in Ref. [9], is likely due to the presence of domains differently orientated with respect to the *top-fcc* configuration, and therefore lying at larger distance from the substrate [11,33] and/or to the presence of subsurface interstitial carbon in the Ni substrate [34]. After the exposure to water, the formation of C–H bonds shifts the C atoms directly involved in the bonding out of the Gr plane, which assume the sp^3 geometry, whereas the surrounding C–Ni bonds get reinforced and the Gr–Ni distance is somewhat reduced. For *top-fcc* Gr/Ni(111) covered by 0.25 ML_{Gr} of H, which is the saturation coverage estimated by XPS, the d value found by DFT calculations remains basically unchanged with respect to clean Gr (see Figure S4 and Ref. [35]). The CTRs in Fig. 3 indicate that d changes by −0.12 Å in the water dosed sample, which can be explained by considering that, in the presence of differently oriented Gr domains, the structure relaxation following the formation of C–H bonds impacts on the Gr-Ni distance [36]. Relevant in this context is that the exposure of Gr/Ni(111) to water shifts the CTR minimum towards lower L values, which undoubtedly excludes that Gr moves away from the substrate, as it would be in the case of intercalation. Hence, this further demonstrates that water dissociation initiates at Gr and not below Gr, in agreement with the insight provided by the C1s spectra.

Additional information about the dissociation route is provided by STM. Fig. 4 shows the images acquired on the clean Gr/Ni(111) surface and after the exposure to water at RT. Fig. 4a shows the hexagonal lattice of Gr grown on Ni(111). The dispersed adatoms, distributed irregularly on the surface, are assumed to be Ni single atoms

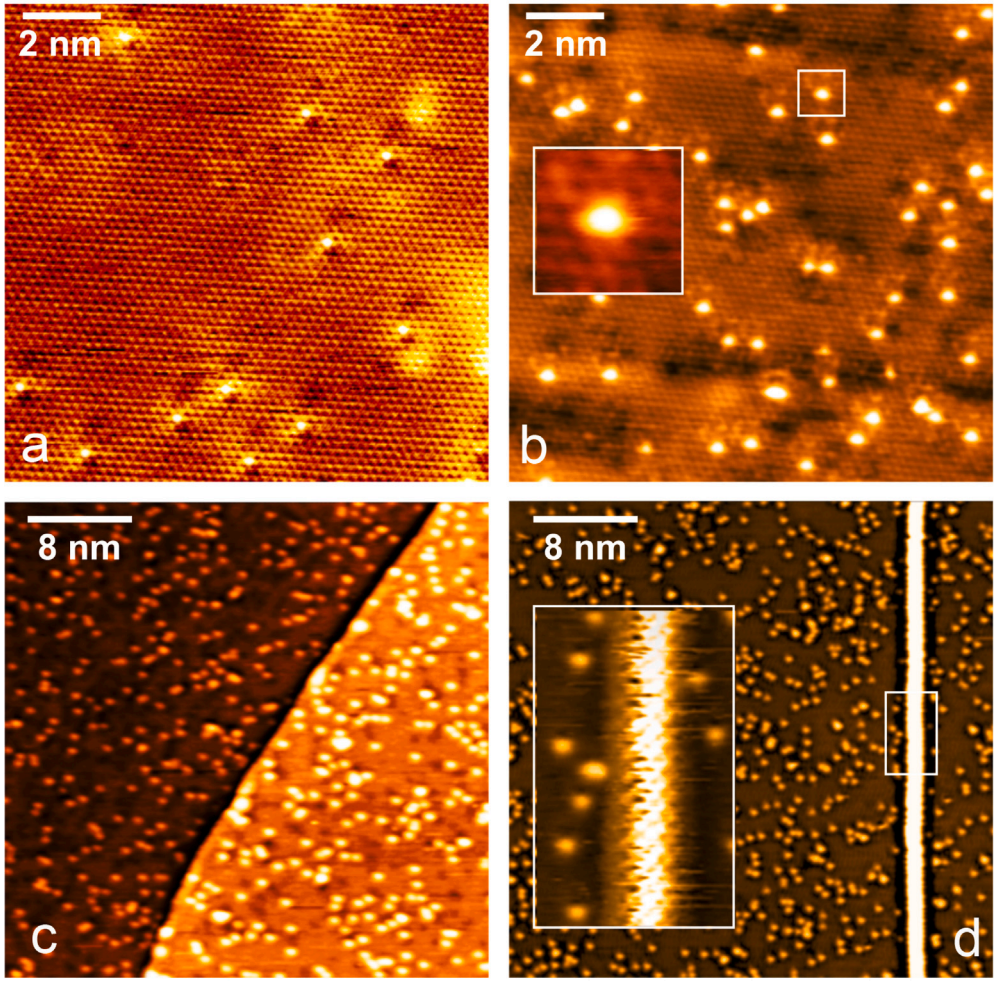

Fig. 4. STM characterization of the Gr/Ni(111) surface before and after exposure to water. (a) Image of the Gr honeycomb lattice with a few nanostructures, likely Ni adatoms trapped at C vacancies (0.08 V, 0.9 nA); (b–d) images of the Gr layer covered by H atoms after the exposure to $\omega_d = 4.5 \times 10^{-3}$ ML of water [(b) 0.46 V, 1.74 nA, inset: 0.46 V, 2.1 nA; (c) 0.44 V, 0.18 nA, (d) (f) 0.68 V, 0.28 nA, inset: 0.68 V, 0.7 nA]. The graphene layer is evenly covered by H atoms in the vicinity of (c) a step edge and (d) a Gr wrinkle, which remains H-free.

trapped in correspondence of C vacancies [37], which, as it will be discussed below, might play an important role in the dissociation of water molecules. The images displayed in Figures 4b-d were acquired after the exposure to $\omega_d = 4.5 \times 10^{-3}$ ML of water and show the continuous Gr layer evenly covered by H atoms, whose surface density increases with water dose (see Figure S5). The H distribution remains fully homogeneous even in the proximity of the step edge (Fig. 4c) or in the vicinity of a Gr wrinkle (Fig. 4d), which strongly hints that water dissociation occurs on the basal plane of Gr/Ni(111). In the images shown in Fig. 4 and Figure S5, the presence of brighter and slightly larger nanostructures, usually accompanied by dimmer features and of dark spots in the surroundings of the H atoms can be noted. We tentatively identify the bright protrusions as trapped Ni adatoms neighbored by H atoms. As for the dark spots the attribution is unclear. On the one hand they could be interpreted as OH groups residing close to their H counterparts. Even if hydroxyls are not detected in the XPS spectra of the sample dosed with 0.02 ML of water, as discussed below, we cannot exclude their presence on the surface exposed to lower water doses. On the other hand, as it can be seen in Fig. 4a, there are dark spots also in the pristine sample, before water dosing, which would indicate that they are not necessarily related to the water dissociation. In this second interpretation, since the Gr lattice appears to be intact, defects could be located in the underlying Ni surface, resulting in a variation in the local density of states, which is probed by STM.

The movie in the Supporting Information demonstrates the manipulation of H atoms by the STM tip. A voltage pulse from −1.2 to 1.5 V was applied while scanning the tip over the bright features, successfully moving those marked by the blue cross. However, the atom highlighted by the green square remained fixed in its position. This suggests that, despite the similar appearance, it may belong to a different species. The most probable explanation is that the movable bright features are hydrogen atoms, while the one which does not move is a Ni atom trapped in the Gr layer.

The experimental results can be summarized by concluding that the initial stage of the interaction of water with Gr/Ni(111) proceeds through dissociative chemisorption occurring on the Gr basal plane, which renders Gr evenly covered by H atoms, whereas the OH counterparts are somehow removed from the Gr surface. However, for completeness it is worth pointing out that a different behavior is observed for an incomplete Gr layer, where the terraces are surrounded by bare substrate areas and the C atoms at the margin of the Gr domains are bound to the Ni atoms. In this case (see Figure S6), after a water dose of only 0.2 ML (see Figure S7) the O1s spectrum shows the presence of OH and O fragments, likely trapped at the dangling bonds terminating the terraces, whereas the C1s spectrum, in addition to the spectral features due to hydrogenation, shows a little C_1 component, indicative of the initial decoupling of Gr from the substrate. Likely, the island edges act as favorable dissociation sites and once terminated by water fragments, might allow the facile diffusion of intact water molecules below graphene [23,38], where they decompose [12].

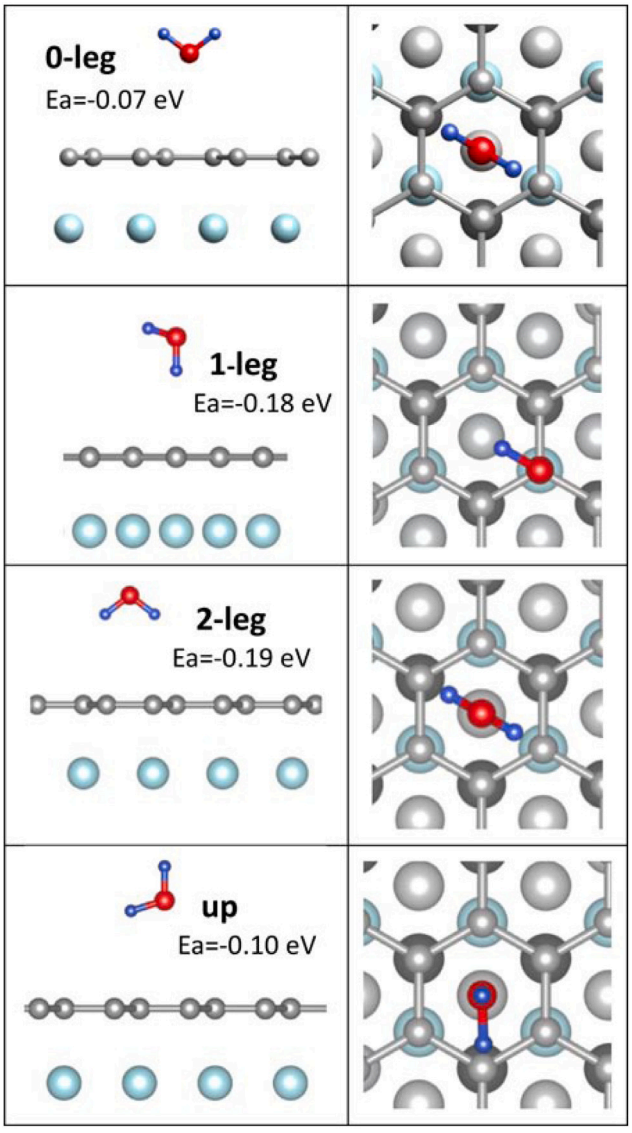

Fig. 5. Adsorption configurations of a water molecule on the Gr/Ni(111) surface shown with the calculated adsorption energies. From top to bottom: 0-*leg*: water molecule located over the center of a Gr hexagon with the two H pointing away from graphene; 1-*leg*: one OH bond nearly perpendicular to the surface (in this case over a C atom in the *top* site), with the other H atom pointing up towards the center of the hexagon; 2-*leg*: water molecule located over the center of a hexagon with the two H pointing down, equidistant from C atoms; *up*: one OH bond nearly vertical over the center of the hexagon and the other H atom pointing down towards a C atom in *fcc* or *top* site. C, H and O atoms are represented with gray, blue and red colors, respectively. Ni atoms in the first, second and third crystal layer from the top appear in order light blue, light gray and dark gray. (A colour version of this figure can be viewed online.)

3.2. Energetics of single water molecule dissociation

In the following we evaluate the energetics of the adsorption and dissociation of water molecules on Gr/Ni(111) by DFT calculations. The configurations taken into account for the adsorption of the water molecule are the same usually considered in the case of free standing Gr, i.e. the 0-*leg*, 1-*leg*, 2-*leg* and *up* geometries that are illustrated and defined in Fig. 5. For H_2O/Gr the adsorption energy E_a reported in the literature for the different configurations are quite similar and range between −70 and −99 meV [39–41], with a slight preference for the 2-*leg* geometry, or, as it has been reported more recently [42], between −110 and −130 meV, with the *up* configuration being the most favorable.

The presence of the Ni substrate stabilizes to some extent the water molecules adsorbed in the 2-*leg* configuration (E_a = −0.19 eV) or in the 1-*leg* configuration with the OH bond on the C atom in the *top* site (E_a = −0.18 eV). The *up* configuration turns out to be energetically slightly less favorable (E_a = −0.10 eV) both with the O-H bond pointing towards the C atom in the *fcc* site and in the *top* site. The 0-*leg* configuration (E_a = −0.07 eV) remains the most weakly bonded even in the presence of the Ni substrate. Therefore, the metal substrate mitigates the hydrophobicity of Gr, that tends to become polarized due to the transfer of the Ni charge (0.08 Mulliken charge per C atom [43]) and then interacts with water through dispersive as well as polar forces. However, the calculated adsorption energies indicate that even if the supporting Ni substrate provides some water wettability, it is not effective in rendering the isolated water molecule stably adsorbed on Gr at room temperature.

Before moving to the dissociative water adsorption, we calculated the adsorption energies of H and OH fragments on Gr/Ni(111). In the following H and OH bonded to the C atoms sitting on Ni in *fcc* and *top* sites are indicated in order as H_{fcc}, OH_{fcc}, H_{top} and OH_{top}. The adsorption energies of −2.42 and −1.83 eV calculated in Ref. [28] for H_{fcc} and H_{top}, respectively, are much lower than E_a on free standing graphene (∼−0.8 eV [44,45]). Also for OH, E_a on Gr/Ni(111) results much more energetically convenient than on plain Gr, decreasing from ∼−0.5 eV calculated for OH/Gr [46,47] to −2.56 and −2.05 eV for OH_{fcc} and OH_{top} on Gr/Ni(111), respectively (see Figure S8). As on bare graphene, [46–48] even in the presence of the Ni substrate the most stable OH configuration is with the C–O bond nearly perpendicular to the Gr plane and the H atom pointing towards the center of the hexagon (see Figure S8). For both H and OH adsorbates the out–of–plane buckling results in a change from the sp^2 to the sp^3 hybridization for the bonding C atom. With respect to plain Gr, in both cases the charge available in the Ni *d*-band compensates the unpaired electron produced when bonding individual H or OH adsorbates, which then turn out to be stabilized [10].

When moving on to the dissociative adsorption of water on Gr/Ni(111), the energetics strongly depends on the stability of the final configuration adopted by OH and H fragments (see Figure S9). It comes out that the configurations with OH and H in *ortho* geometry (see scheme at the right-top corner in Fig. 6) are the least stable, with the same E_a = 1.3 eV regardless of the *fcc* or *top* site occupied by each fragment, whereas the *meta* and *para* geometries are more stable with OH_{fcc}. The most stable configuration with E_a = 0.77 eV has H_{fcc} and OH_{fcc} in *meta* geometry (see Fig. 6), with the axis of the OH group slightly rotated away from the C–H bond, and the two C atoms bonded to H and OH lifted by 0.50 Å above the Gr plane. On free-standing Gr the most thermodynamically favorable configuration with both H and OH on the same surface side has the adsorbates in *ortho* position and E_a = 2.57 eV [49]. Then, the presence of the Ni substrate somehow stabilizes the final dissociative state. However, the dissociative adsorption of an isolated water molecule remains an endothermic process incompatible with the prominent water splitting yield observed experimentally.

In the following we explore the possibility that the dissociation of a single water molecule on Gr/Ni(111) could be made easier by the presence of adsorbates, lattice defects or structural discontinuities. On bare graphene water dissociation is reported to be facilitated by pre-adsorbed H or OH species. A pre-adsorbed H atom was calculated to lower the dissociative adsorption energy by nearly 1 eV [49] and, accordingly, it was found that the dissociation energy barrier of water on graphene, calculated to be of the order of 3.64 eV, [3] is lowered to 3.34 eV in the presence of a pre-adsorbed OH [50]. Then, also for the dissociation on Gr/Ni(111) we calculated how pre-adsorbed H atoms affect the energetics of specific final configurations. For the most stable H_{fcc}–OH_{fcc} configuration in *meta* geometry identified above, one pre-adsorbed H_{fcc} atom decreases E_a from 0.77 eV to −1.60 eV (Fig. 6). The pre-adsorbed H induces a sp^3 character in the flat Gr

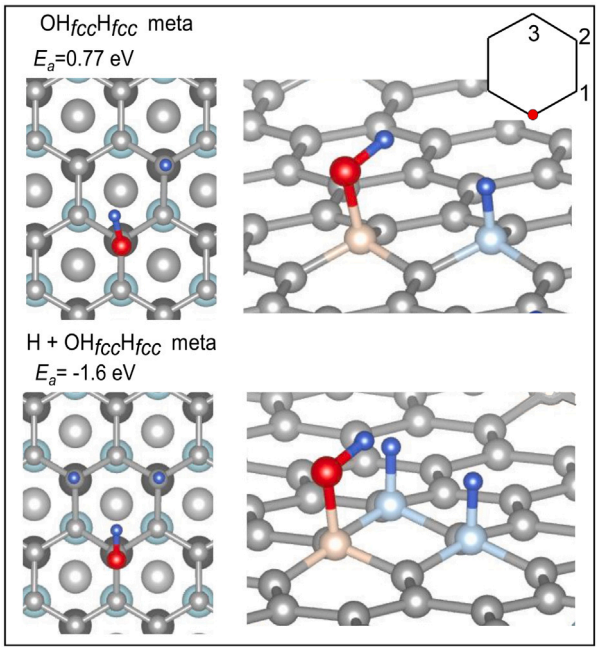

Fig. 6. Top and side view of a dissociated water molecule on Gr/Ni(111), with both H and OH fragments bonded to C atoms in *fcc* sites. The configuration with a pre-adsorbed H_{fcc} atom is shown in the bottom panels. C, H and O atoms are represented with gray, blue and red colors, respectively. Ni atoms in the first, second and third crystal layer from the top appear in order light blue, light gray and dark gray. For a better visualization of the graphene buckling, in the right column images the Ni crystal has been removed and the C atoms bonded to O and H are colored in light pink and light blue, respectively. The scheme in the right-top corner shows the *ortho* (1), *meta* (2) and *para* (3) positions with respect to the vertex marked by the red dot. (A colour version of this figure can be viewed online.)

layer enhancing the local reactivity, as it has been observed in the case of h-BN [51]. Analogously, for the H_{fcc}–OH_{top} configuration in *ortho* geometry, which is the most favorable for water dissociation on plain Gr, a single pre-adsorbed H_{fcc} atom lowers E_a from 1.27 to −1.18 eV (Figures S7a and S7j). Hence, having a H atom pre-adsorbed on Gr renders the water dissociation exothermic. However, it turns out that the H_2O molecule approaching the Gr surface with a pre-adsorbed H_{fcc} atom must overcome an energy barrier E_b of 2.27 eV to dissociate (first row of Fig. 7 and Fig. 8). In the final state H and OH chemisorb at two adjacent sites forming a $OH_{top}H_{fcc}$ *ortho* configuration. This reaction path is by far more energetically favorable than reaching the slightly more exothermic $OH_{fcc}H_{fcc}$ *meta* configuration, because of the shorter distance between the H and OH adsorption sites. Anyhow, the calculated high E_b value prevents the occurrence of spontaneous water splitting at RT, even in the presence of pre-adsorbed H atoms in the surrounding. Even if the final state is energetically convenient it cannot be reached without the support of external energy.

A further possibility to assist the molecule dissociation could be provided by lattice defects. For bare graphene, water splitting appears substantially easier in correspondence of vacancy sites, where dissociative chemisorption is calculated to occur with an energy barrier of only 0.4 −0.7 eV [42,50,52] or even less [3]. In order to explore this possibility also in the case of Gr/Ni(111), one C atom was removed from the Gr layer producing a mono-vacancy in *fcc* (V_{fcc}) or in *top* (V_{top}) sites. Among the possible final states with H and OH saturating two of the three C dangling bonds surrounding the vacancy, the most stable configuration (E_a = −2.6 eV) resulted V_{top} with H and OH bonded to two *fcc* C atoms facing the empty C site (Fig. 7h). This final state is slightly endothermic in comparison to the initial state, where the water molecule is physisorbed in the vicinity of the defect (E_a = −2.93 eV; Fig. 7e), and can be reached after overcoming an energy barrier of 1.5 eV (see middle row in Fig. 7 and Fig. 8), which, however, is still too high to allow spontaneous water splitting at RT.

A stronger substrate reactivity is obtained when the C vacancy is filled with a Ni atom. For Gr/Ni(111) it has been shown that, during the CVD growth, Ni atoms can be trapped in correspondence of C mono-vacancies or larger defects sites [37], where they might behave as active sites for catalytic reactions [53–55]. Interestingly, the barrier for water dissociation on bare Gr has been calculated to decrease from 5.13 to 1.52 eV (0.58–1.09 eV) by Ni (Zn, Cu, Fe, Co) [50] single atom catalysts (SACs) in the Gr lattice [56]. Even if a systematic analysis of all possible geometries for Ni atoms trapped at multi-atom vacancies is beyond the scope of this study, we have considered whether a Ni atom saturating the three C dangling bonds of a C mono-vacancy in the *top* ($Ni@V_{top}$) or in the *fcc* site ($Ni@V_{fcc}$) could effectively catalyze water splitting. In the two geometries Ni stays 0.8 Å above [37] or 0.6 Å below (see Fig. 7i) the Gr plane, respectively.

We found that the most favorable configuration for the dissociated water is obtained with the $Ni@V_{fcc}$ structure. In this case, in the final state H and OH are bonded to two C atoms neighboring the Ni dopant (Fig. 7l) and is exothermic by −0.8 eV with respect to having the intact molecule far from the substrate (Fig. 7i). The energy barrier encountered by the water molecule to undergo dissociation is 0.8 eV, with the transition state corresponding to the molecule almost parallel to the surface (bottom row in Fig. 7 and Fig. 8). This value, much lower than E_b = 1.52 eV calculated for the analogous system without the Ni substrate [50], can be compatible with RT dissociation at a reasonable rate for water molecules impinging on Gr/Ni(111). Further DFT studies may find out whether Ni SACs trapped at different defect sites such as double C vacancies [37] or Stone–Wales-like defects would catalyze the water splitting reaction more effectively. For $Ni@V_{fcc}$, the energy gained in the reaction can be used by the H and OH fragments to diffuse away from the defect site, that then remains free to catalyze new dissociation reactions. Hence, even if the Ni substrate below Gr cannot induce the dissociation of isolated water molecules on the Gr basal plane, the reaction can anyhow occur in correspondence of Ni trapped at C vacancies. The limited surface density (~0.01 ML_{Gr}) of these defects, which decreases with the Gr growth temperature [37], might not account for the H coverage of ~0.25 ML_{Gr} observed by XPS, but the capability of the Ni SACs to initiate the splitting reaction locally, might be fundamental in the overall process.

Actually, on several metal and non-metal substrates the adsorption energy of water molecules is lowered and the dissociation rate enhanced when they bind to surface hydroxyls. It has been proposed that these autocatalytic reactions [57–60] are triggered by the H-bond which forms in the OH-H_2O complex and might modify adsorption, desorption and dissociation kinetics. Near ambient pressure experiments [57–59] have shown that surface OH groups capable of trapping H_2O molecules govern the surface chemistry by increasing residence time and promoting autocatalytic dissociation of water molecules. By analogy, we can suppose that also at the dosing pressure used in this experiment, similar autocatalytic reactions, triggered by the OH groups initially produced by the Ni SACs, could contribute to achieve the observed water dissociation yield. For this reaction to occur, it would be necessary to have contiguous free C sites, available for the adsorption of H and OH. Our DFT calculations found that water dissociation is inhibited in the presence of two H atoms occupying two C_{fcc} sites of the same lattice hexagon where the H_2O fragments are going to chemisorb (see Figure S9l), which would set the H coverage of ~0.25 ML as the limit beyond which dissociation becomes unfavorable. More important, in this study we have considered the energetics of single water molecule dissociation leaving out the impact of cooperative effects, that can lower the dissociation energy barrier of water molecules adsorbing as dimers or larger clusters [61–63].

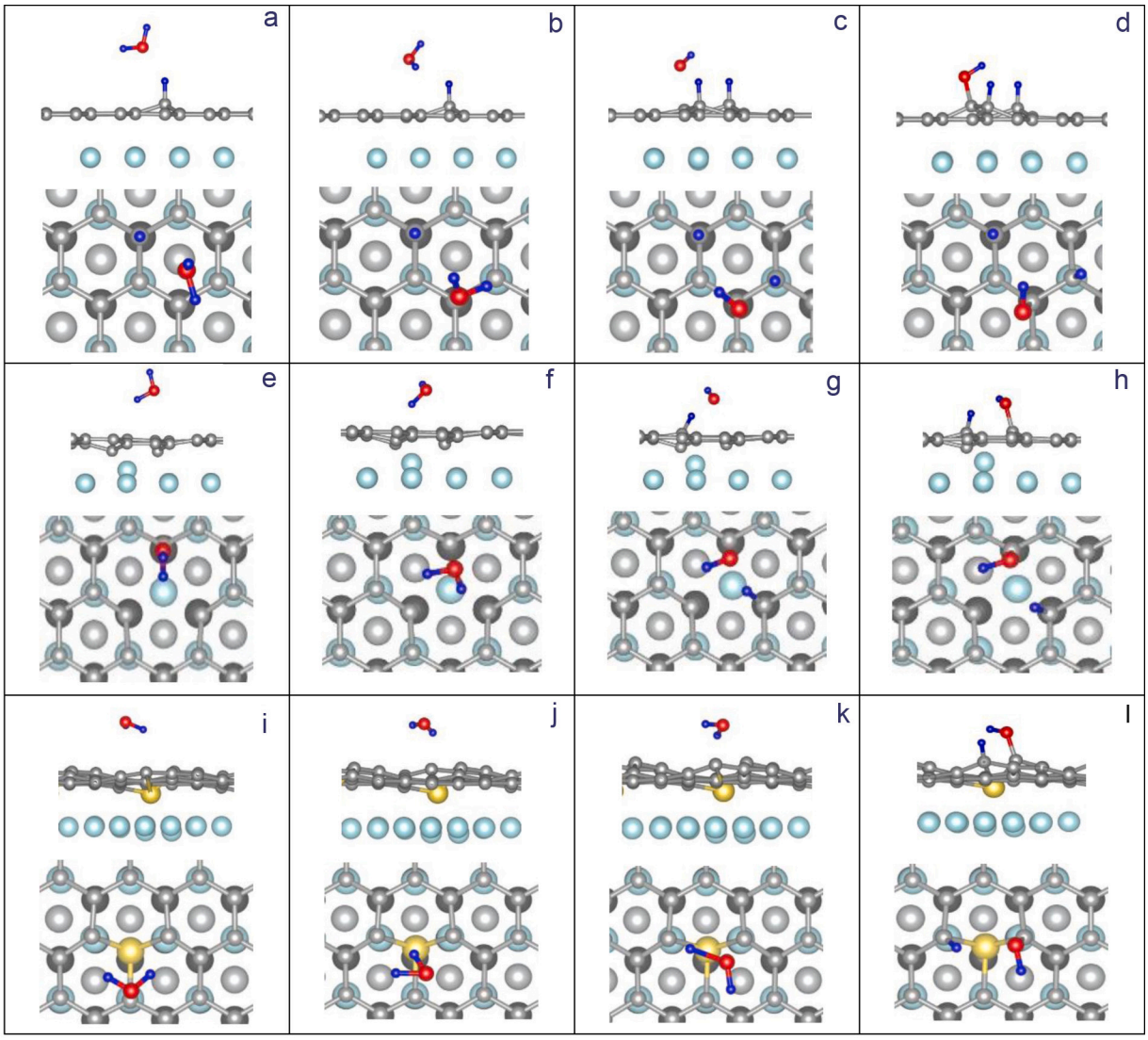

Fig. 7. Dissociative chemisorption of water on the Gr/Ni(111) surface in the presence of (a–d) a pre-adsorbed H_{fcc} atom, (e–h) a C vacancy in the *top* site (V_{top}) and (i–l) a C vacancy in the *fcc* site filled by a Ni atom ($Ni@V_{fcc}$). The side and top view of the different interface configurations during water dissociation are illustrated in each case. In each panel C, H, O atoms and Ni SACs are represented with gray, blue, red and yellow colors, respectively. Ni atoms in the first, second and third crystal layer from the top appear light blue, light gray and dark gray, respectively. (A colour version of this figure can be viewed online.)

3.3. Hydroxyl desorption

The other aspect worth discussing is the lack of O-containing species on the Gr surface at low water doses. As noted above (see Fig. 1), when exposing the Gr/Ni(111) surface to water doses up to 1.9 ML, whereas H atoms appear stably bonded to graphene, in the O1s spectra there is no evident trace of hydroxyl OH groups (nor of O atoms) bonded to the Gr/Ni(111) interface. A similar absence of hydroxyl groups has been reported for the splitting of water molecules on the $Fe_3O_4(0001)$ magnetite surface [64].

We attribute the lack of OH species to the occurrence of reactions either between hydroxyls bonded to graphene and/or following the interaction with impinging H_2O molecules. A first possible reaction pathway is the recombination of two hydroxyls into a hydrogen peroxide H_2O_2 molecule [65]

$$OH_{ads} + OH_{ads} \rightarrow H_2O_2 \uparrow \quad (1)$$

or even into H_2 and O_2 molecules [64]

$$OH_{ads} + OH_{ads} \rightarrow H_2 \uparrow + O_2 \uparrow \quad (2)$$

However, in both cases the reactions would require the diffusion of at least one hydroxyl group on graphene. In this respect it is important to notice that, whereas OH can diffuse quite freely on plain graphene with an energy barrier of ~0.3 eV [47], we calculated that on Gr/Ni(111) the E_b for the shift from OH_{top} to OH_{fcc} site is 0.67 eV, and that the inverse path requires to overcome an energy barrier of 1.17 eV (see Figure S8). Hence, although single $OH_{top} \rightarrow OH_{fcc}$ displacements are possible, longer path are unfeasible at RT without the support of extra energy. Consequently, the reactions between adsorbed hydroxyls appear quite unfavorable. However, the formation of H bonds between surface OH and adsorbing H_2O molecules could effectively weaken the OH-substrate bonds decreasing the OH diffusion barrier [66]. Furthermore, H_2O molecules interacting with surface hydroxyls could originate desorbing hydrogen peroxide molecules leaving H atoms bonded to Gr

$$OH_{ads} + H_2O_{gas} \rightarrow H_2O_2 \uparrow + H_{ads} \quad (3)$$

whereas a different pathway suggested in Ref. [10] would include the full dissociation of a first water molecule, the subsequent reaction of the adsorbed epoxide oxygen with a second water molecule to produce

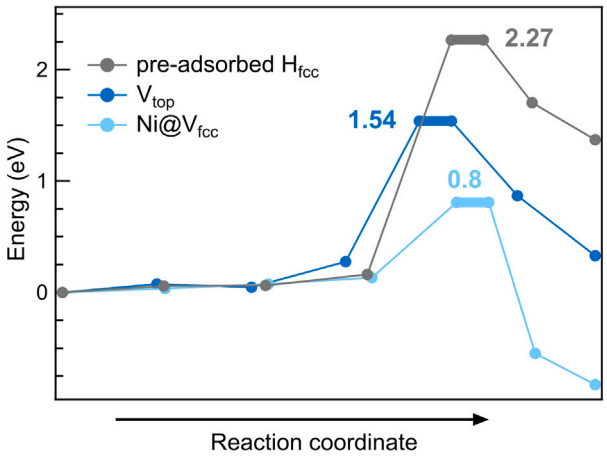

Fig. 8. Calculated energy barriers for the three routes of water dissociation on Gr/Ni(111) illustrated in Fig. 7, namely in the presence of (gray curve) a pre-adsorbed H_{fcc} atom, (blue curve) a C vacancy in the *top* site (V_{top}) and (cyan curve) a C vacancy in the *fcc* site filled by a Ni atom (Ni@V_{fcc}). (A colour version of this figure can be viewed online.)

a proton and a peroxide group OOH, which then desorbs as O_2 leaving a new H atom on Gr:

$$H_2O_{gas} \rightarrow O_{ads} + 2H_{ads} \quad (4)$$

$$O_{ads} + H_2O_{gas} \rightarrow OOH_{ads} + H_{ads} \rightarrow O_2 \uparrow + 2H_{ads} \quad (5)$$

These reactions, which could be energetically unfavorable if considered as isolated events, can be facilitated by the presence of nearby adsorbates and/or the participation of multiple water molecules, that can change the charge configuration at the reaction site modifying dissociation and recombination rates [67,68].

As reported above, when exposing the incomplete Gr layer on Ni(111) to water, there are O and OH species detected by XPS after a water dose of 0.2 ML (see Figure S7). The TPD curves shown in Figure S7c indicate desorption temperatures of 350 and 400 K for OH and O fragments [69], i.e. adsorption energies as low as ~1 eV [70]. Moreover, both fragments progressively disappear after higher water doses, most likely being removed through the interaction with incoming water molecules. For complete Gr, where the density of defects anchoring the hydroxyls is by far lower, the analogous OH removal is expected to be more effective and, possibly, already completed during the lowest water exposure we tested and therefore undetected by XPS. Likely, in the very first stage of the water interaction with Gr/Ni(111), when the molecules start to impact on the clean graphene surface, dissociation at the trapped Ni SACs and possibly autocatalytic or cooperatively supported dissociation reactions are the main reaction channels, which yield both H and OH fragments bound to Gr. Then, after prolonged exposure to water, the low availability of surface sites renders the dissociation reaction less competitive, while reactions (3–5) turn predominant and hydroxyl groups become fewer and fewer on the surface. Notably, adsorbed H atoms, which have much less probability to be removed by the incoming H_2O molecule, tend to permanently occupy the surface sites and progressively outnumber the OH adsorbates. The hypotheses described here can be confirmed or refuted by further, well-planned experiments. By systematically varying sample temperature and water dosing pressure in appropriate ranges, it should be possible to obtain conclusive information on the role of the temperature in the dissociation reaction and establish the real importance of collective effects. Furthermore, once the hydroxyls are revealed, a proper modulation of the experimental parameters would certainly allow to identify the mechanism that determines their disappearance.

4. Conclusion

The first stage of water adsorption on Gr/Ni(111) at room temperature was experimentally investigated by combining XPS, TPD, surface diffraction and STM. The results indicate the occurrence of Gr hydrogenation while no O-containing species were detected by XPS. The combination of chemical, structural and microscopy measurements demonstrate that initially the dissociation occurs on the basal plane of graphene, without the need for water molecules to intercalate below to get in contact with the metal substrate. When heating the sample dosed with water, H_2 molecules are released at a temperature of approximately 600 K. The energetics of the dissociation of a single water molecule on the clean Gr/Ni(111) surface, and in the presence of pre-adsorbed H atoms or of Gr lattice defects, were evaluated by DFT calculations. In comparison to bare graphene, the presence of the Ni substrate limits the Gr hydrophobicity, slightly increases the stability of physisorbed water molecules and decreases the adsorption energy of dissociated molecules, which however remains positive. In the presence of pre-adsorbed H atoms and C mono-vacancy defects, water dissociation becomes exothermic, but the energy barriers remain too high to be afforded at RT without the support of external energy. On the contrary, Ni atoms trapped at C vacancies catalyze the dissociation reaction rendering the activation energy compatible with a reasonable reaction rate at RT. In this case, the energy released in the reaction can ease fragment diffusion, leaving the surrounding of the Ni catalyst available for new splitting events. However, due to the limited number of single Ni atoms catalysts in the Gr layer, collective adsorption processes or autocatalytic dissociative reactions seem to be largely responsible for the extensive water dissociation occurring at RT. The interaction of water molecules with H and OH adsorbates primarily remove surface hydroxyls leaving only H atoms bonded to Gr. Following the surface reactions for water doses much lower than those used here can shed light on the kinetics of formation and removal of adsorbed hydroxyls. Additional experiments carried out as a function of dosing pressure and temperature could better elucidate the water dissociation mechanism and allow the optimization of the experimental parameters which maximize hydrogen production.

CRediT authorship contribution statement

Monica Pozzo: Writing – review & editing, Validation, Investigation, Funding acquisition. **Paolo Lacovig:** Writing – review & editing, Software, Investigation, Data curation. **Marco Bianchi:** Writing – review & editing, Investigation. **Monika Schied:** Writing – review & editing, Investigation. **Luca Bignardi:** Writing – review & editing, Investigation. **Francesca Zarotti:** Writing – review & editing, Investigation. **Roberto Felici:** Writing – review & editing, Validation, Supervision, Investigation. **Dario Alfè:** Writing – review & editing, Funding acquisition. **Silvano Lizzit:** Writing – review & editing, Validation, Investigation. **Rosanna Larciprete:** Writing – review & editing, Writing – original draft, Investigation, Funding acquisition, Conceptualization.

Declaration of competing interest

The authors declare that they have no known competing financial interests or personal relationships that could have appeared to influence the work reported in this paper.

Acknowledgments

D.A. and R.L. acknowledge the Italian Ministero dell'Università e della Ricerca for the support of the PRIN Project No. 20222FXZ33. F.Z., R.F. and R.L. acknowledge funding from Lazio Innova/Regione Lazio (Grant No. 85-2017-15316). MP acknowledges the funding from the DOME 4.0 project from the European Union's Horizon 2020 Research and Innovation Programme under Grant Agreement No. 953163. The authors acknowledge Elettra Sincrotrone Trieste for providing access to its synchrotron radiation facilities and for financial support.

Appendix A. Supplementary data

Supplementary material related to this article can be found online at https://doi.org/10.1016/j.carbon.2025.120422.

References

[1] K. Pomerantseva, F. Bonaccorso, X. Feng, Y. Cui, Y. Gogotsi, Energy storage: The future enabled by nanomaterials, Science 366 (2019) eaan8285, http://dx.doi.org/10.1126/science.aan8285.

[2] P.A. Denis, Chemical reactivity of electron-doped and hole-doped graphene, J. Phys. Che, C 117 (8) (2013) 3895–3902, http://dx.doi.org/10.1021/jp306544m.

[3] Z. Xu, Z. Ao, D. Chu, A. Younis, C.M. Li, S. Li, Reversible hydrophobic to hydrophilic transition in graphene via water splitting induced by UV irradiation, Sci. Rep. 4 (2014) 6450, http://dx.doi.org/10.1038/srep06450.

[4] A. Ambrosetti, P.L. Silvestrelli, Communication: Enhanced chemical reactivity of graphene on a Ni(111) substrate, J. Chem. Phys. 144 (11) (2016) 111101, http://dx.doi.org/10.1063/1.4944090.

[5] C. Zhang, B.-J. Lee, H. Li, J. Samdani, T.-H. Kang, J.-S. Yu, Catalytic mechanism of graphene-nickel interface dipole layer for binder free electrochemical sensor applications, Commun. Chem. 1 (2018) 94, http://dx.doi.org/10.1038/s42004-018-0088-x.

[6] H.-J. Qiu, Y. Ito, W. Cong, Y. Tan, P. Liu, A. Hirata, T. Fujita, Z. Tang, M. Chen, Nanoporous graphene with single-atom nickel dopants: An efficient and stable catalyst for electrochemical hydrogen production, Angew. Chem. Int. Ed. 54 (47) (2015) 14031–14035, http://dx.doi.org/10.1002/anie.201507381.

[7] E.N. Voloshina, A. Generalov, M. Weser, S. Böttcher, K. Horn, Y.S. Dedkov, Structural and electronic properties of the graphene/Al/Ni(111) intercalation system, New J. Phys. 13 (11) (2011) 113028, http://dx.doi.org/10.1088/1367-2630/13/11/113028.

[8] J. Lahiri, T.S. Miller, A.J. Ross, L. Adamska, I.I. Oleynik, M. Batzill, Graphene growth and stability at nickel surfaces, New J. Phys. 13 (2) (2011) 025001, http://dx.doi.org/10.1088/1367-2630/13/2/025001.

[9] R. Rameshan, V. Vonk, D. Franz, J. Drnec, S. Penner, A. Garhofer, F. Mittendorfer, A. Stierle, K. Bernhard, Role of precursor carbides for graphene growth on Ni(111), Sci. Rep. 8 (2018) 2662, http://dx.doi.org/10.1038/s41598-018-20777-4.

[10] D.W. Boukhvalov, Y.-W. Son, R.S. Ruoff, Water splitting over graphene-based catalysts: Ab initio calculations, ACS Catal. 4 (6) (2014) 2016–2021, http://dx.doi.org/10.1021/cs5002288.

[11] P.L. Silvestrelli, A. Ambrosetti, Van der Waals corrected DFT simulation of adsorption processes on transition-metal surfaces: Xe and graphene on Ni(111), Phys. Rev. B 91 (2015) 195405, http://dx.doi.org/10.1103/PhysRevB.91.195405.

[12] A. Politano, M. Cattelan, D.W. Boukhvalov, D. Campi, A. Cupolillo, S. Agnoli, N.G. Apostol, P. Lacovig, S. Lizzit, D. Farías, G. Chiarello, G. Granozzi, R. Larciprete, Unveiling the mechanisms leading to H_2 production promoted by water decomposition on epitaxial graphene at room temperature, ACS Nano 10 (4) (2016) 4543–4549, http://dx.doi.org/10.1021/acsnano.6b00554.

[13] T. Pache, H.-P. Steinrück, W. Huber, D. Menzel, The adsorption of H_2O on clean and oxygen precovered ni(111) studied by ARUPS and TPD, Surf. Sci. 224 (1) (1989) 195–214, http://dx.doi.org/10.1016/0039-6028(89)90910-2.

[14] T.E. Madey, F.P. Netzer, The adsorption of H_2O on Ni(111); influence of preadsorbed oxygen on azimuthal ordering, Surf. Sci. 117 (1) (1982) 549–560, http://dx.doi.org/10.1016/0039-6028(82)90537-4.

[15] P.M. Hundt, B. Jiang, M.E. van Reijzen, H. Guo, R.D. Beck, Vibrationally promoted dissociation of water on Ni(111), Science 344 (6183) (2014) 504–507, http://dx.doi.org/10.1126/science.1251277.

[16] P. Feulner, D. Menzel, Simple ways to improve flash desorption measurements from single crystal surfaces, J. Vac. Sci. Technol. 17 (1980) 662–663, http://dx.doi.org/10.1116/1.570537.

[17] G. Kresse, J. Furthmüller, Efficient iterative schemes for ab initio total-energy calculations using a plane-wave basis set, Phys. Rev. B 54 (1996) 11169–11186, http://dx.doi.org/10.1103/PhysRevB.54.11169.

[18] I. Hamada, Van der Waals density functional made accurate, Phys. Rev. B 89 (2014) 121103, http://dx.doi.org/10.1103/PhysRevB.89.121103.

[19] P.E. Blöchl, Projector augmented-wave method, Phys. Rev. B 50 (1994) 17953–17979, http://dx.doi.org/10.1103/PhysRevB.50.17953.

[20] J.P. Perdew, K. Burke, M. Ernzerhof, Generalized gradient approximation made simple, Phys. Rev. Lett. 77 (1996) 3865–3868, http://dx.doi.org/10.1103/PhysRevLett.77.3865.

[21] G. Henkelman, B.P. Uberuaga, H. Jónsson, A climbing image nudged elastic band method for finding saddle points and minimum energy paths, J. Chem. Phys. 113 (22) (2000) 9901–9904, http://dx.doi.org/10.1063/1.1329672.

[22] A. Dahal, M. Batzill, Graphene–nickel interfaces: a review, Nanoscale 6 (2014) 2548–2562, http://dx.doi.org/10.1039/C3NR05279F.

[23] L.L. Patera, C. Africh, R.S. Weatherup, R. Blume, S. Bhardwaj, C. Castellarin-Cudia, A. Knop-Gericke, R. Schloegl, G. Comelli, S. Hofmann, C. Cepek, In situ observations of the atomistic mechanisms of Ni catalyzed low temperature graphene growth, ACS Nano 7 (2013) 7901–7912, http://dx.doi.org/10.1021/nn402927q.

[24] G. Petrone, F. Zarotti, P. Lacovig, D. Lizzit, E. Tosi, R. Felici, S. Lizzit, R. Larciprete, The effect of structural disorder on the hydrogen loading into the graphene/nickel interface, Carbon 199 (2022) 357–366, http://dx.doi.org/10.1016/j.carbon.2022.07.050.

[25] C. Africh, C. Cepek, L.L. Patera, G. Zamborlini, P. Genoni, T.O. Menteş, A. Sala, A. Locatelli, G. Comelli, Switchable graphene-substrate coupling through formation/dissolution of an intercalated Ni-carbide layer, Sci. Rep. 6 (2016) 19734, http://dx.doi.org/10.1038/srep19734.

[26] D. Haberer, D.V. Vyalikh, S. Taioli, B. BoukDora, M. Farjam, J. Fink, D. Marchenko, T. Pichler, K. Ziegler, S. Simonucci, M.S. Dresselhaus, M. Knupfer, B. Büchner, A. Grüneis, Tunable band gap in hydrogenated quasi-free-standing graphene, Nano Lett. 10 (9) (2010) 3360–3366, http://dx.doi.org/10.1021/nl101066m.

[27] D. Lizzit, M.I. Trioni, L. Bignardi, P. Lacovig, S. Lizzit, R. Martinazzo, R. Larciprete, Dual-route hydrogenation of the graphene/Ni interface, ACS Nano 13 (2) (2019) 1828–1838, http://dx.doi.org/10.1021/acsnano.8b07996.

[28] M. Pozzo, T. Turrini, L. Bignardi, P. Lacovig, D. Lizzit, E. Tosi, S. Lizzit, A. Baraldi, D. Alfè, R. Larciprete, Interplay among hydrogen chemisorption, intercalation, and bulk diffusion at the graphene-covered Ni(111) crystal, J. Phys. Chem. C 127 (14) (2023) 6938–6947, http://dx.doi.org/10.1021/acs.jpcc.3c00291.

[29] J. Yeh, I. Lindau, At. Data Nucl. Data Tables 32 (1985) 1–155.

[30] J. Yeh, Atomic Calculation of Photoionization Cross-Sections and Asymmetry Parameters, Gordon and Breach Science Publishers, Langhorne, PE (USA), 1993.

[31] M.L. Ng, R. Balog, L. Hornekær, A.B. Preobrajenski, N.A. Vinogradov, N. Mårtensson, K. Schulte, Controlling hydrogenation of graphene on transition metals, J. Phys. Chem. C 114 (43) (2010) 18559–18565, http://dx.doi.org/10.1021/jp106361y.

[32] L. Hornekær, V. Šljivančanin, W. Xu, R. Otero, E. Rauls, I. Stensgaard, E. Lægsgaard, B. Hammer, F. Besenbacher, Metastable structures and recombination pathways for atomic hydrogen on the graphite (0001) surface, Phys. Rev. Lett. 96 (2006) 156104, http://dx.doi.org/10.1103/PhysRevLett.96.156104.

[33] M. Hasegawa, K. Nishidate, T. Hosokai, N. Yoshimoto, Electronic-structure modification of graphene on Ni(111) surface by the intercalation of a noble metal, Phys. Rev. B 87 (2013) 085439, http://dx.doi.org/10.1103/PhysRevB.87.085439.

[34] S.C. Matysik, C. Papp, A. Görling, Solving the puzzle of the coexistence of different adsorption geometries of graphene on Ni(111), J. Phys. Chem C 122 (45) (2018) 26105–26110, http://dx.doi.org/10.1021/acs.jpcc.8b09438.

[35] W. Zhao, J. Gebhardt, F. Späth, K. Gotterbarm, C. Gleichweit, H.-P. Steinrück, A. Görling, C. Papp, Reversible hydrogenation of graphene on Ni(111)—synthesis of graphone, Chem. Eur. J. 21 (8) (2015) 3347–3358, http://dx.doi.org/10.1002/chem.201404938.

[36] L. Kyhl, R. Balog, A. Cassidy, J. Jørgensen, A. Grubisic-Čabo, L. Trotochaud, H. Bluhm, L. Hornekær, Enhancing graphene protective coatings by hydrogen-induced chemical bond formation, ACS Appl. Nano Mater. 1 (9) (2018) 4509–4515, http://dx.doi.org/10.1021/acsanm.8b00610.

[37] V. Carnevali, L.L. Patera, G. Prandini, M. Jugovac, S. Modesti, G. Comelli, M. Peressi, C. Africh, Doping of epitaxial graphene by direct incorporation of nickel adatoms, Nanoscale 11 (2019) 10358–10364, http://dx.doi.org/10.1039/C9NR01072F.

[38] G. He, Q. Wang, H.K. Yu, D. Farías, Y. Liu, A. Politano, Water-induced hydrogenation of graphene/metal interfaces at room temperature: Insights on water intercalation and identification of sites for water splitting, Nano Res. 12 (2019) 3101–3108, http://dx.doi.org/10.1007/s12274-019-2561-y.

[39] J. Ma, A. Michaelides, D. Alfè, L. Schimka, G. Kresse, E. Wang, Adsorption and diffusion of water on graphene from first principles, Phys. Rev. B 84 (2011) 033402, http://dx.doi.org/10.1103/PhysRevB.84.033402.

[40] J.G. Brandenburg, A. Zen, M. Fitzner, B. Ramberger, G. Kresse, T. Tsatsoulis, A. Grüneis, A. Michaelides, D. Alfè, Physisorption of water on graphene: Subchemical accuracy from many-body electronic structure methods, J. Phys. Chem Lett. 10 (3) (2019) 358–368, http://dx.doi.org/10.1021/acs.jpclett.8b03679.

[41] E. Voloshina, D. Usvyat, M. Schütz, Y. Dedkov, B. Paulus, On the physisorption of water on graphene: a CCSD(T) study, Phys. Chem. Chem. Phys. 13 (25) (2011) 12041, http://dx.doi.org/10.1039/c1cp20609e.

[42] Z. Liang, K. Li, Z. Wang, Y. Bu, J. Zhang, Adsorption and reaction mechanisms of single and double H_2O molecules on graphene surfaces with defects: a density functional theory study, Phys. Chem. Chem. Phys. 23 (2021) 19071–19082, http://dx.doi.org/10.1039/D1CP02595C.

[43] J. Liu, C.-Y. Lai, Y.-Y. Zhang, M. Chiesa, S.T. Pantelides, Water wettability of graphene: interplay between the interfacial water structure and the electronic structure, RSC Adv. 8 (2018) 16918–16926, http://dx.doi.org/10.1039/C8RA03509A.

[44] L. Hornekær, E. Rauls, W. Xu, V. Šljivančanin, R. Otero, I. Stensgaard, E. Lægsgaard, B. Hammer, F. Besenbacher, Clustering of chemisorbed H(D) atoms on the graphite (0001) surface due to preferential sticking, Phys. Rev. Lett. 97 (2006) 186102, http://dx.doi.org/10.1103/PhysRevLett.97.186102.

[45] S. Casolo, O.M. Løvvik, R. Martinazzo, G.F. Tantardini, Understanding adsorption of hydrogen atoms on graphene, J. Chem. Phys. 130 (5) (2009) 054704, http://dx.doi.org/10.1063/1.3072333.

[46] B. Grosjean, C. Pean, A. Siria, L. Bocquet, R. Vuilleumier, M.-L. Bocquet, Chemisorption of hydroxide on 2D materials from DFT calculations: Graphene versus hexagonal boron nitride, J. Phys. Chem. Lett. 7 (22) (2016) 4695–4700, http://dx.doi.org/10.1021/acs.jpclett.6b02248.

[47] N. Ghaderi, M. Peressi, First-principle study of hydroxyl functional groups on pristine, defected graphene, and graphene epoxide, J. Phys. Chem. C 114 (49) (2010) 21625–21630, http://dx.doi.org/10.1021/jp108688m.

[48] M. Barhoumi, D. Rocca, M. Said, S. Lebègue, A first principle study of graphene functionalized with hydroxyl, nitrile, or methyl groups, J. Chem. Phys. 146 (4) (2017) 044705, http://dx.doi.org/10.1063/1.4974894.

[49] Y.S. Al-Hamdani, D. Alfè, O.A. von Lilienfeld, A. Michaelides, Tuning dissociation using isoelectronically doped graphene and hexagonal boron nitride: Water and other small molecules, J. Chem. Phys. 144 (15) (2016) 154706, http://dx.doi.org/10.1063/1.4945783.

[50] L. Yang, X. Li, G. Zhang, P. Cui, X. Wang, X. Jiang, J. Zhao, Y. Luo, J. Jiang, Combining photocatalytic hydrogen generation and capsule storage in graphene based sandwich structures, Nat. Comm. 8 (2017) 16049, http://dx.doi.org/10.1038/ncomms16049.

[51] A. Siria, P. Poncharal, A.-L.A. Biance, R. Fulcrand, X. Blase, S.T. Purcell, L. Bocquet, Giant osmotic energy conversion measured in a single transmembrane boron nitride nanotube, Nature 494 (2013) 455–458, http://dx.doi.org/10.1038/nature11876.

[52] P. Cabrera-Sanfelix, G.R. Darling, Dissociative adsorption of water at vacancy defects in graphite, J. Phys. Chem. C 111 (49) (2007) 18258–18263, http://dx.doi.org/10.1021/jp076241b.

[53] L. Zhang, Y. Jia, G. Gao, X. Yan, N. Chen, J. Chen, M.T. Soo, B. Wood, D. Yang, A. Du, X. Yao, Graphene defects trap atomic Ni species for hydrogen and oxygen evolution reactions, Chem 4 (2) (2018) 285–297, http://dx.doi.org/10.1016/j.chempr.2017.12.005.

[54] A. Baby, L. Trovato, C. Di Valentin, Single atom catalysts (SAC) trapped in defective and nitrogen-doped graphene supported on metal substrates, Carbon 174 (2021) 772–788, http://dx.doi.org/10.1016/j.carbon.2020.12.045.

[55] D. Perilli, V. Chesnyak, A. Ugolotti, M. Panighel, S. Vigneri, F. Armillotta, P. Naderasli, M. Stredansky, M. Schied, P. Lacovig, S. Lizzit, C. Cepek, G. Comelli, H. Brune, C. Africh, C. Di Valentin, CO adsorption on a single-atom catalyst stably embedded in graphene, Angew. Chem. Int. Ed. 64 (11) (2025) e202421757, http://dx.doi.org/10.1002/anie.202421757.

[56] X. Guo, S. Liu, S. Huang, Single Ru atom supported on defective graphene for water splitting: DFT and microkinetic investigation, Int. J. Hydrog. Energy 43 (10) (2018) 4880–4892, http://dx.doi.org/10.1016/j.ijhydene.2018.01.122.

[57] K. Andersson, G. Ketteler, H. Bluhm, S. Yamamoto, H. Ogasawara, L.G.M. Pettersson, M. Salmeron, A. Nilsson, Bridging the pressure gap in water and hydroxyl chemistry on metal surfaces: the Cu(110) case, J. Phys. Chem. C 111 (39) (2007) 14493–14499, http://dx.doi.org/10.1021/jp073681u.

[58] K. Andersson, G. Ketteler, H. Bluhm, S. Yamamoto, H. Ogasawara, L.G.M. Pettersson, M. Salmeron, A. Nilsson, Autocatalytic water dissociation on Cu(110) at near ambient conditions, J. Am. Chem. Soc. 130 (9) (2008) 2793–2797, http://dx.doi.org/10.1021/ja073727x.

[59] J.T. Newberg, D.E. Starr, S. Yamamoto, S. Kaya, T. Kendelewicz, E.R. Mysak, S. Porsgaard, M.B. Salmeron, G.E. Brown, A. Nilsson, H. Bluhm, Autocatalytic surface hydroxylation of MgO(100) terrace sites observed under ambient conditions, J. Phys. Chem. C 115 (26) (2011) 12864–12872, http://dx.doi.org/10.1021/jp200235v.

[60] D. Donadio, L.M. Ghiringhelli, L. Delle Site, Autocatalytic and cooperatively stabilized dissociation of water on a stepped platinum surface, J. Am. Chem. Soc. 134 (2012) 19217–19222, http://dx.doi.org/10.1021/ja308899g.

[61] M. Odelius, Mixed molecular and dissociative water adsorption on MgO[100], Phys. Rev. Lett. 82 (19) (1999) 3919–3922, http://dx.doi.org/10.1103/physrevlett.82.3919.

[62] K. Akagi, M. Tsukada, Theoretical study of the hydrogen relay dissociation of water molecules on Si(001) surfaces, Surf. Sci. 438 (1–3) (1999) 9–17, http://dx.doi.org/10.1016/s0039-6028(99)00538-5.

[63] C. Michel, F. Göltl, P. Sautet, Early stages of water/hydroxyl phase generation at transition metal surfaces – synergetic adsorption and O–H bond dissociation assistance, Phys. Che, Che, Phys. 14 (44) (2012) 15286, http://dx.doi.org/10.1039/c2cp43014b.

[64] G.S. Parkinson, Z. Novotný, P. Jacobson, M. Schmid, U. Diebold, Room temperature water splitting at the surface of magnetite, J. Am. Chem. Soc. 133 (32) (2011) 12650–12655, http://dx.doi.org/10.1021/ja203432e.

[65] B. Chen, Y. Xia, R. He, H. Sang, W. Zhang, J. Li, L. Chen, P. Wang, S. Guo, N.Y. Yi, L. Hu, M. Song, Y. Liang, Y. Wang, G. Jiang, R. Zare, Water-solid contact electrification causes hydrogen peroxide production from hydroxyl radical recombination in sprayed microdroplets., PNAS 119 (2022) e2209056119, http://dx.doi.org/10.1073/pnas.2209056119.

[66] D.W. Boukhvalov, Modeling of hydrogen and hydroxyl group migration on graphene, Phys. Chem. Chem. Phys. 12 (47) (2010) 15367, http://dx.doi.org/10.1039/c0cp01009j.

[67] S. Du, J.S. Francisco, S. Kais, Study of electronic structure and dynamics of interacting free radicals influenced by water, J. Chem. Phys. 130 (12) (2009) 124312, http://dx.doi.org/10.1063/1.3100549.

[68] J. Lee, K. Walker, H. Han, J. Kang, F. Prinz, R. Waymouth, H. Nam, R. Zare, Spontaneous generation of hydrogen peroxide from aqueous microdroplets, PNAS 24 (2019) 19294–19298, http://dx.doi.org/10.1073/pnas.1911883116.

[69] J.B. Romero, O. Chavez, C. Rodriguez, S. Gonzalez, J. Fregoso, V. Carbajal, G. Clavel, O. Hudak, J. Cheng, J. Tandoc, J. Brown, L. Gao, Water dissociation on graphene/Ir(111) studied by temperature-dependent x–ray photoelectron spectroscopy, MRS Adv. 9 (2024) 1176–1182, http://dx.doi.org/10.1557/s43580-024-00866-5.

[70] P.A. Redhead, Thermal desorption of gases, Vacuum 12 (1962) 203–211, http://dx.doi.org/10.1016/0042-207X(62)90978-8.